



저작자표시-비영리-변경금지 2.0 대한민국

이용자는 아래의 조건을 따르는 경우에 한하여 자유롭게

- 이 저작물을 복제, 배포, 전송, 전시, 공연 및 방송할 수 있습니다.

다음과 같은 조건을 따라야 합니다:



저작자표시. 귀하는 원저작자를 표시하여야 합니다.



비영리. 귀하는 이 저작물을 영리 목적으로 이용할 수 없습니다.



변경금지. 귀하는 이 저작물을 개작, 변형 또는 가공할 수 없습니다.

- 귀하는, 이 저작물의 재이용이나 배포의 경우, 이 저작물에 적용된 이용허락조건을 명확하게 나타내어야 합니다.
- 저작권자로부터 별도의 허가를 받으면 이러한 조건들은 적용되지 않습니다.

저작권법에 따른 이용자의 권리는 위의 내용에 의하여 영향을 받지 않습니다.

이것은 [이용허락규약\(Legal Code\)](#)을 이해하기 쉽게 요약한 것입니다.

[Disclaimer](#)

Master of Science

**ASSESSMENT OF ADHESION AND TRIBOLOGY
CHARACTERISTICS OF CHROMIUM-BASED DIAMOND
COATING FOR PISTON RING**

The Graduation School of the University of Ulsan

School of Mechanical Engineering

Vu Nga Linh

**ASSESSMENT OF ADHESION AND TRIBOLOGY
CHARACTERISTICS OF CHROMIUM-BASED DIAMOND
COATING FOR PISTON RING**

Supervisor: Professor **Koo-Hyun Chung**

A Thesis

Submitted to the School of Mechanical Engineering and the Graduate School

of University of Ulsan, Republic of Korea

in partial fulfillment of the requirements

for the degree of Master of Science in Mechanical Engineering

by

Vu Nga Linh

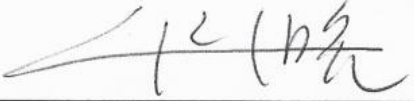
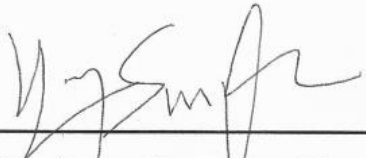

School of Mechanical Engineering

University of Ulsan, Republic of Korea

December 2020

**ASSESSMENT OF ADHESION AND TRIBOLOGY
CHARACTERISTICS OF CHROMIUM-BASED DIAMOND
COATING FOR PISTON RING**

This certifies that the dissertation
of Vu Nga Linh is approved.

Committee Chairman	 Professor Doo-Man Chun
Committee Member	 Professor Sung-Tae Hong
Committee Member	 Professor Koo-Hyun Chung

School of Mechanical Engineering
University of Ulsan, Republic of Korea

December 2020

ACKNOWLEDGEMENTS

Firstly, I would like to express my gratitude to my advisor, Professor Koo-Hyun Chung, for his support, encouragement, and guidance throughout this research. Without his kind-hearted support, I would never have the present results.

And I am very grateful for the guidance and support of all my laboratory members (Tribology and Surface Engineering Laboratory, University of Ulsan) when I have a hard time working.

Finally, and most importantly, I would like to thank my parents, family, and Vietnamese friends who always support and encourage me in my life, which is my great driving force in implementing this thesis.

ABSTRACT

Assessment of Adhesion and Tribology Characteristics of Chromium-Based Diamond Coating for Piston Ring

Vu Nga Linh

School of Mechanical Engineering

The Graduate School

University of Ulsan

Recently, the use of chromium-based diamond coating on the piston ring's running surface has remarkable attention due to its sound friction reduction and wear resistance to improve the lifetime of the piston ring. The piston ring's adhesion and tribology characteristics with chromium-based diamond coating on grey cast iron and ductile cast iron as a base material were investigated using scratch test and pin-on-reciprocating test in this work. The chromium steel ball was used as counterpart sliding against piston ring specimens in the wear test. The results showed that the work of adhesion, friction coefficient, and wear rate of piston ring with base material of ductile cast iron was better than of grey cast iron. Compared with grey cast iron, the work of adhesion of ductile cast iron and coating increased by 66%. The friction coefficient in the case of ductile cast iron was slightly smaller than that of grey cast iron. The wear rate of the piston ring with ductile cast iron was reduced by up to 36% at 40 N of normal force compared to grey cast iron. The outcomes of this work showed the promising applications of chromium-based diamond coating on ductile cast iron of piston ring in the field condition.

Keywords: piston ring, coating, work of adhesion, friction coefficient, wear rate.

TABLE OF CONTENTS

ACKNOWLEDGEMENTS	i
ABSTRACT	ii
TABLE OF CONTENTS	iii
LIST OF FIGURES.....	iv
1. INTRODUCTION.....	1
1.1 Background and motivation.....	1
1.2 Objective of thesis.....	6
1.3 Organization of thesis	6
2. MATERIALS AND METHODS	7
2.1 Materials	7
2.2 Methods.....	13
2.2.1 <i>Scratch adhesion test</i>	13
2.2.2 <i>Pin-on-reciprocating test</i>	15
3. RESULTS AND DISCUSSION	19
3.1 Adhesion characteristics	19
3.2 Tribology characteristics.....	23
4. CONCLUSIONS	33
REFERENCES	35

LIST OF FIGURES

Figure 1. Structure of Cr-diamond coating (www.federalmogul.com).....	5
Figure 2. Some failure modes in the scratch test (www.federalmogul.com).....	5
Figure 3. Cross-sectional images of specimens (a) A and (b) B, SEM images of interface of specimens (c) A and (d) B, (e) hardness, (f) load-displacement curve of coating, (g) porosity of coating, images of surface of specimens (h) A and (i) B corresponding with cross-sectional profile, (j) three-dimensional images of specimens A and B.	10
Figure 4. Photograph of (a) scratch adhesion tester, scratch specimen, indenter, and three-dimensional image of indenter, (b) pin-on-reciprocating tribo-tester, plate specimen, pin specimen and three-dimensional of the Cr steel ball.....	18
Figure 5. Optical images corresponding with cross-sectional profile of scratch track formed on specimens and friction profile of (a) specimen A and (b) specimen B, (c) failure modes, (d) work of adhesion.....	22
Figure 6. The friction coefficient with respect to number of cycles of different normal force of two specimens (a) A, (b) B and (c) at an average value of different normal forces.	24
Figure 7. (a) Optical images corresponding with cross-sectional profile of wear formed on the Cr steel balls before and after test with different normal force, (b) wear volume, (c) wear rate of balls respect to normal force.	26
Figure 8. (a) Optical images corresponding with cross-sectional profile of wear tracks formed on the plates with different normal force, (b) wear volume, (c) wear rate of plates respect to normal force.....	29

Figure 9. (a) Optical image wear tracks formed on the specimen B under 30 N of normal force, (b) high-resolution optical image of worn surface of the ball sliding against specimen B under 30 N of normal force. 32

1. INTRODUCTION

1.1 Background and motivation

A piston ring is a critical component of an internal combustion engine, which is appended to the grooves on the outer surface. The piston ring has the following functions: sealing the distance between the piston and the cylinder liner to minimize the loss of compression pressure to the crankcase, ensuring the amount of lubricant to smooth the up and down motion, and dissipating the accumulated heat inside the piston to the cylinder wall to avoid the engine damage [1]. Therefore, the piston rings' tribological behavior is an essential factor affecting the internal combustion engine's performance in terms of power loss, fuel consumption, and emissions [2]. The largest part of friction losses in the engine was at piston assembly from the literature survey, responsible for 45-55% of the energy loss from the engine friction [3]. Reducing fuel consumption and emission by improving engine efficiency is always a challenge to internal combustion engine designers and manufacturers. Several methods have been proposed to reduce the friction loss of the piston ring-cylinder liner pair, such as lubrication improvement, mechanical design, and surface modification [4]. Coatings are among the most common surface treatments for tribological applications to provide lower friction and wear resistance for sliding tribo-pair.

Nowadays, various coating techniques have been applied to the running surface of the piston ring. Among all, chromium-based coatings are good candidates for research and development. They can increase sliding components' lives due to their outstanding low friction characteristics and good wear resistance [5]. Numerous studies to evaluate

the properties and performance of chromium-based coating for piston rings have been conducted, such as chromium-plated (Cr) [6], CrN [7], Cr-Al₂O₃ [8]. A representative of chromium-based coating developed by Federal-Mogul Powertrain LLC is GDC-Goetze diamond coating (Cr-diamond), which gives consistent performance against too high stresses in the engine [9]. Cr-diamond coating is chromium coating reinforced with micro-diamond particles embedded in the extremely fine crack network coated on the piston rings' outer surface by the electrochemical deposition method, whose structure is shown in Fig. 1. Li et al. compared the friction and wear capabilities of piston ring coatings: Cr, PVD, PCVD, and GDC. The results indicate that the GDC coating shows a minimum wear rate and the lowest friction coefficient, while the Cr coating shows the least resistance to friction and wear. The wear rate of the GDC ring is only 15% of the chromium ring [10]. Wan et al.'s research also indicated that a Cr-diamond ring has better advantages over Cr and Cr- Al₂O₃ rings. Performance is related to hardness enough to withstand extreme pressure and phase transition from diamond to graphite types to deal with poor lubrication conditions [11].

However, the current studies only focus on the friction reduction and wear resistance of Cr-diamond coating without analyzing the bond between Cr-diamond coating and substrates. The fracture strength and the coating's adhesion properties are considered critical intrinsic parameters were determining the coating-substrate system's performance and reliability [12]. Several techniques are used to measure coating adhesion, such as pull-off test, body-force methods, acoustic imaging, laser techniques, indentation, and scratch tests [13]. Among all, the scratch test is a widely used, fast, and effective method to obtain critical loads related to the adhesion properties of coating [5,

12-17]. The raw materials to manufacture piston rings are commonly cast iron or steel [18]. Cast iron has proven its suitability as a piston ring material for marine diesel engines due to its relatively high mechanical strength, good heat resistance properties, and thermal conductivity [19]. Grey cast iron has a dark grey fracture color due to a graphitic microstructure, which is the most common form of cast iron. Ductile cast iron is defined by the presence of graphite in the form of spherical nodules. In this work, the base material considerations are grey cast iron and ductile cast iron.

The types of failure observed in the scratch test depend critically on the properties of both substrate and coating. Suppose the coating is very soft compared to the substrate. In this case, considerable plastic deformation will occur within it, and the scratch test critical load may be defined as the load at which the coating is scraped off, exposing the substrate. However, it is not always easy to determine when this has occurred, and quantifying the failure mode is challenging. For a hard coating on a softer substrate, spallation and buckling failure modes resulting from interfacial detachment and a range of other cracks and deformed regions can be observed. Both the spallation and buckling failure modes are amenable to quantification. This case is suitable for the coating-substrate system in this work. For hard coatings on hard substrates, the failure is occasionally observed to coincide with the coating-substrate interface, but this is not always the case, making the test results difficult to interpret. Thus, if scratch testing is to be used for adhesion assessment, only the spallation and buckling failure modes are beneficial. It generally limits the scratch test to the assessment of hard coatings on softer substrates. However, there is a tendency for the diamond stylus to wear during the test in cases where both substrate and coating are hard, so the test has been most widely applied

to hard coating-soft substrate systems. Fig. 2 shows some failure types of adhesion-related failures are observed in the scratch test [14]:

- Buckle spallation: coating buckles ahead of the stylus tip, irregularly wide arc-shaped patches missing, opening away from the scratch direction.
- Wedge spallation: caused by a delaminated region wedging ahead to separate the coating, regularly spaced annular-circular that extends beyond the edge of the groove.
- Recovery spallation: regions of detached coating along one or both sides of the groove, produced by elastic recovery behind the stylus and plastic deformation in the substrate.
- Gross spallation: large detached regions, common in coating with low adhesion strength.

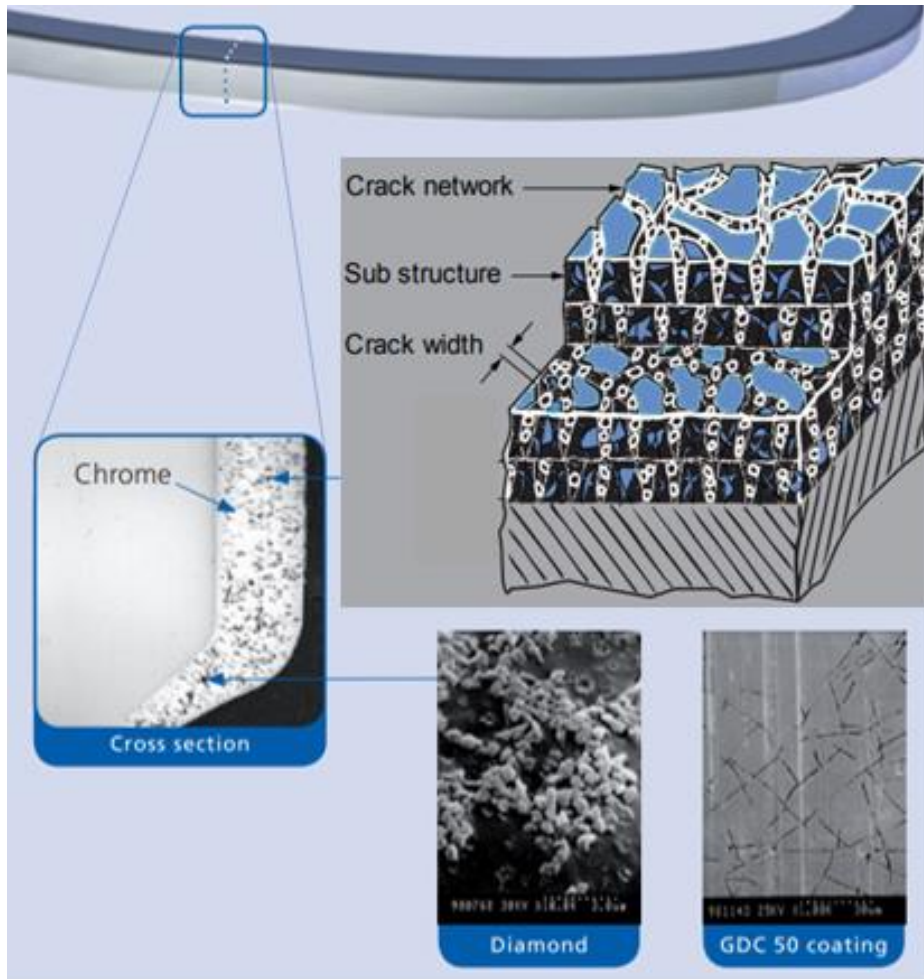


Figure 1. Structure of Cr-diamond coating (www.federalmogul.com)

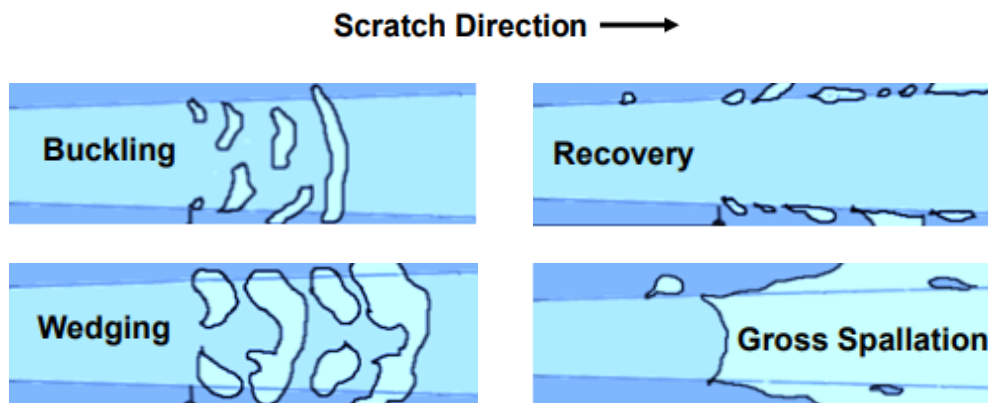


Figure 2. Some failure modes in the scratch test (www.federalmogul.com)

1.2 Objective of thesis

This study aims at investigating the adhesion and tribology characteristics of Cr-diamond coating. The adhesion properties were examined by using a scratch adhesion test. The friction and wear behavior were evaluated using a pin-on-reciprocating tribotester under oil boundary lubrication to simulate the piston ring's actual movement in the cylinder. From the results obtained, the quantitative assessment of the work of adhesion, friction reduction, and wear resistance of Cr-diamond coating was provided. This work's outcomes provide information to help understand the properties of Cr-diamond, therefore providing a useful method to choose the best substrate material and conditions for operation.

1.3 Organization of thesis

The overall structure of this thesis combines four sections. The motivation and objectives of this work have been explained in section 1.

In section 2, the specimen preparation process and experimental setup were described. The adhesion and tribology characteristics of Cr-diamond coated piston ring was investigated by scratch adhesion test and pin-on-reciprocating test.

In section 3, adhesion, friction, and wear behavior obtained from the scratch test, and tribo-test were presented and analyzed.

Finally, the main conclusions of this research are summarized in section 4.

2. MATERIALS AND METHODS

2.1 Materials

Specimens were prepared from two commercial top rings in the four-stroke large-bore ship engines, provided by Federal-Mogul Powertrain LLC, Michigan, USA. The piston rings' dimension has an outer diameter of 330 mm, a width of 8 mm, and a radial wall thickness of 10.5 mm. The piston ring specimens' structure was characterized using a laser scanning confocal microscope (VK-X200, Keyence, Osaka, Japan). Fig. 3(a) and (b) show the images of the cross-sectional structure of specimens A and B. It can be seen from the figure the structure of piston ring specimens is similar. A chromium coating reinforced with micro-diamond particles embedded in the extremely fine crack network was coated on the piston rings' outer surface by the electrochemical deposition method. The thickness of coating layers of specimens A and B are 160 – 200 μm and 145 – 200 μm , respectively. The base materials of specimens A and B are grey cast iron and ductile cast iron, respectively. The cross-sectional structure performs an asymmetrical-curved barreled running surface to secure a good oil film between the piston ring and cylinder. Fig. 3(c) and (d) are the scanning electron microscopy images of the interface between the coatings and the substrates. It can be seen from figures that there are holes or porosity in the interface area. The hardness of coating materials and base materials of specimens are shown in Fig. 3(e). The hardness of coating layers and base materials was measured using a microhardness tester (MMT-7 Micro Vickers Hardness Tester, Matsuzawa, Kawabe, Japan). Hardness indentation was performed on randomly selected five different locations on one cross-section specimen of each specimen at 0.1 kgf with a dwell time of 20 s. The results were determined by using the laser scanning confocal microscope. The

average hardness of the coating layer of specimens A and B is 923 ± 35 HV and 981 ± 14 HV, respectively (mean ± 1 standard deviation). The results show that the hardness of the coating layer on specimens is similar. The values determined from this work agree with the hardness of the Cr-diamond coating from the literature [10, 11]. The average hardness of grey cast iron and ductile cast iron is 348 ± 23 HV and 527 ± 12 HV, respectively (mean ± 1 standard deviation). The hardness of grey cast iron of specimen A is smaller than the hardness of ductile cast iron of specimen B. The elastic modulus of Cr-diamond coating was performed using the nano-indentation method on the coating surface using a Berkovich tip. The maximum indentation force of 3 mN, the loading and unloading rate of 3 mN/min, was applied with the Poisson's ratio of 0.3. More than eight indentations were made on each specimen. The results were calculated using the Oliver Pharr method [19]. The average elastic modulus of Cr-diamond coating of specimens A and B was 256 ± 45 GPa and 269 ± 26 GPa, respectively (mean ± 1 standard deviation). The ultimate tensile strength, elastic modulus, and Brinell hardness of grey cast iron and ductile cast iron are 320 – 440 MPa and 670 – 790 MPa, 110 – 140 GPa and 150 – 180 GPa, 210 – 250 HBN and 240 – 280 HBN, respectively [20]. Therefore, it can be concluded that ductile cast iron's mechanical properties are better than grey cast iron. Fig. 3(f) shows an example of the load-displacement curve resulting from the nano-indentation test of two specimens, which have a similar shape. It was found that the elastic modulus of Cr-diamond coating on specimens is similar. The coating porosity was evaluated by analyzing the laser scanning confocal microscopy data, as shown in Fig. 3(g). As expected, there is a typical high density of microcracks. The coating's porosity is easily calculated based on the percentage of pores and micro-cracks as the black area

and solid material as the white area. The average porosity was evaluated from five different locations on the cross-section with a scan size of $150 \times 150 \mu\text{m} \times \mu\text{m}$ for each specimen. The average porosity of the coating of specimens A and B was $7.19 \pm 0.57 \%$ and $7.18 \pm 0.70 \%$, respectively. It was found that the porosity of the coating of the two specimens was similar. Overall, all results indicated no difference in the coating layers' mechanical properties in the two specimens.

Figure 3(h) and (i) show the image of the surface of the Cr-diamond coating of specimens A and B, along with their cross-sectional profiles by using a laser scanning confocal microscope. As shown in Figs. 3(h) and (i), the surface texturing of coating specimens A and B were modified differently. Crosshatch pattern is honing trace made to retain oil or grease to ensure proper lubrication and ring seal of pistons in cylinders. The crosshatch pattern area on the surface of specimen B is broader than that of specimen A. Fig. 3(j) shows the three-dimensional image of the crosshatch pattern area of the Cr-diamond coating of specimens A and B. The arithmetic average surface roughness of this area of Cr-diamond coating of specimens A and B obtained from laser scanning confocal microscopy data at three locations of five specimens at scan size $1408 \times 1056 \mu\text{m} \times \mu\text{m}$ were determined about $1.37 \pm 0.08 \mu\text{m}$ and $1.17 \pm 0.08 \mu\text{m}$, respectively (mean \pm 1 standard deviation). The results indicate that the surface roughness of the crosshatch pattern area of the Cr-diamond coating of specimens A is slightly higher, about 15 %, than specimen B.

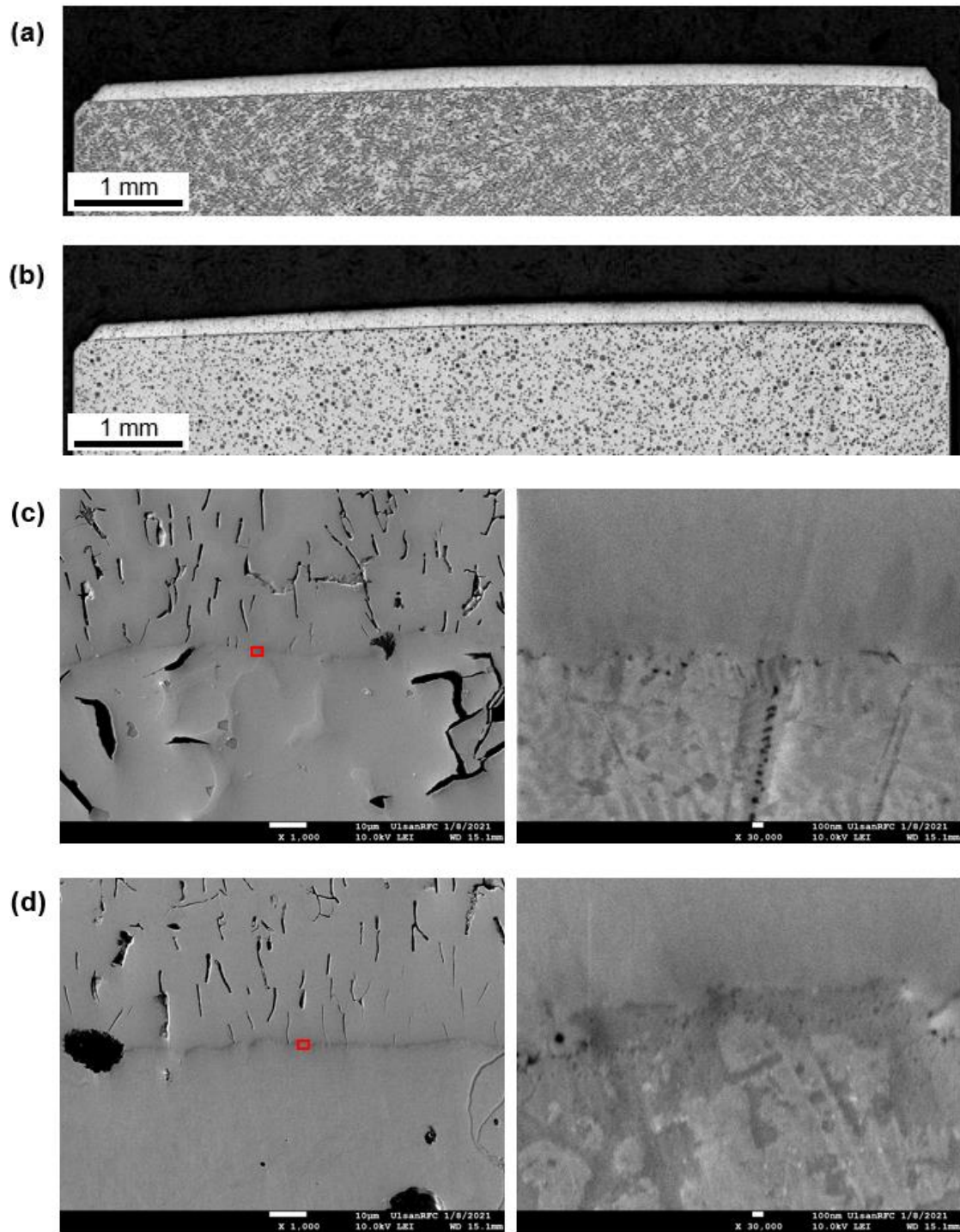


Figure 3. Cross-sectional images of specimens (a) A and (b) B, SEM images of interface of specimens (c) A and (d) B, (e) hardness, (f) load-displacement curve of coating, (g) porosity of coating, images of surface of specimens (h) A and (i) B corresponding with cross-sectional profile, (j) three-dimensional images of specimens A and B.

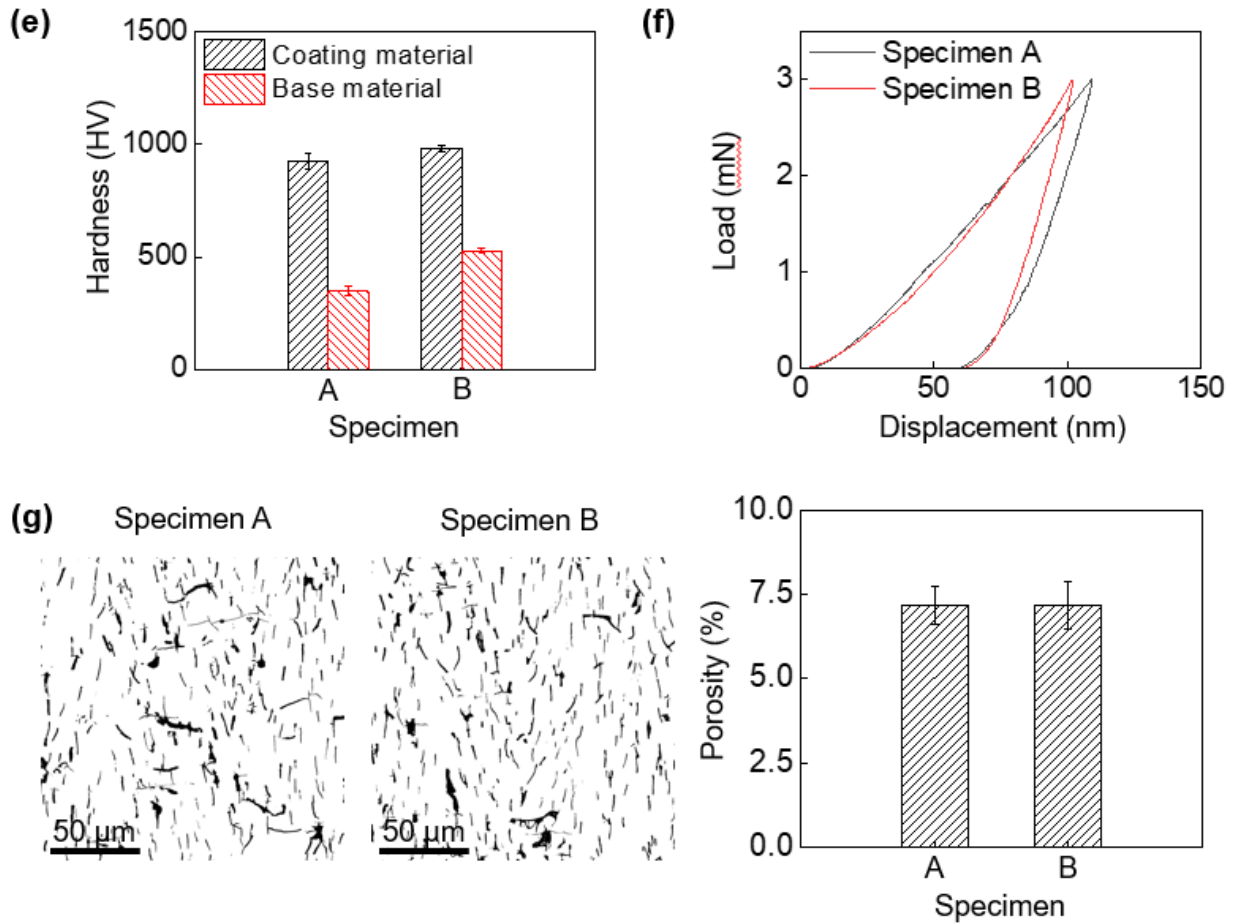


Figure 4. Cross-sectional images of specimens (a) A and (b) B, SEM images of interface of specimens (c) A and (d) B, (e) hardness, (f) load-displacement curve of coating, (g) porosity of coating, images of surface of specimens (h) A and (i) B corresponding with cross-sectional profile, (j) three-dimensional images of specimens A and B.

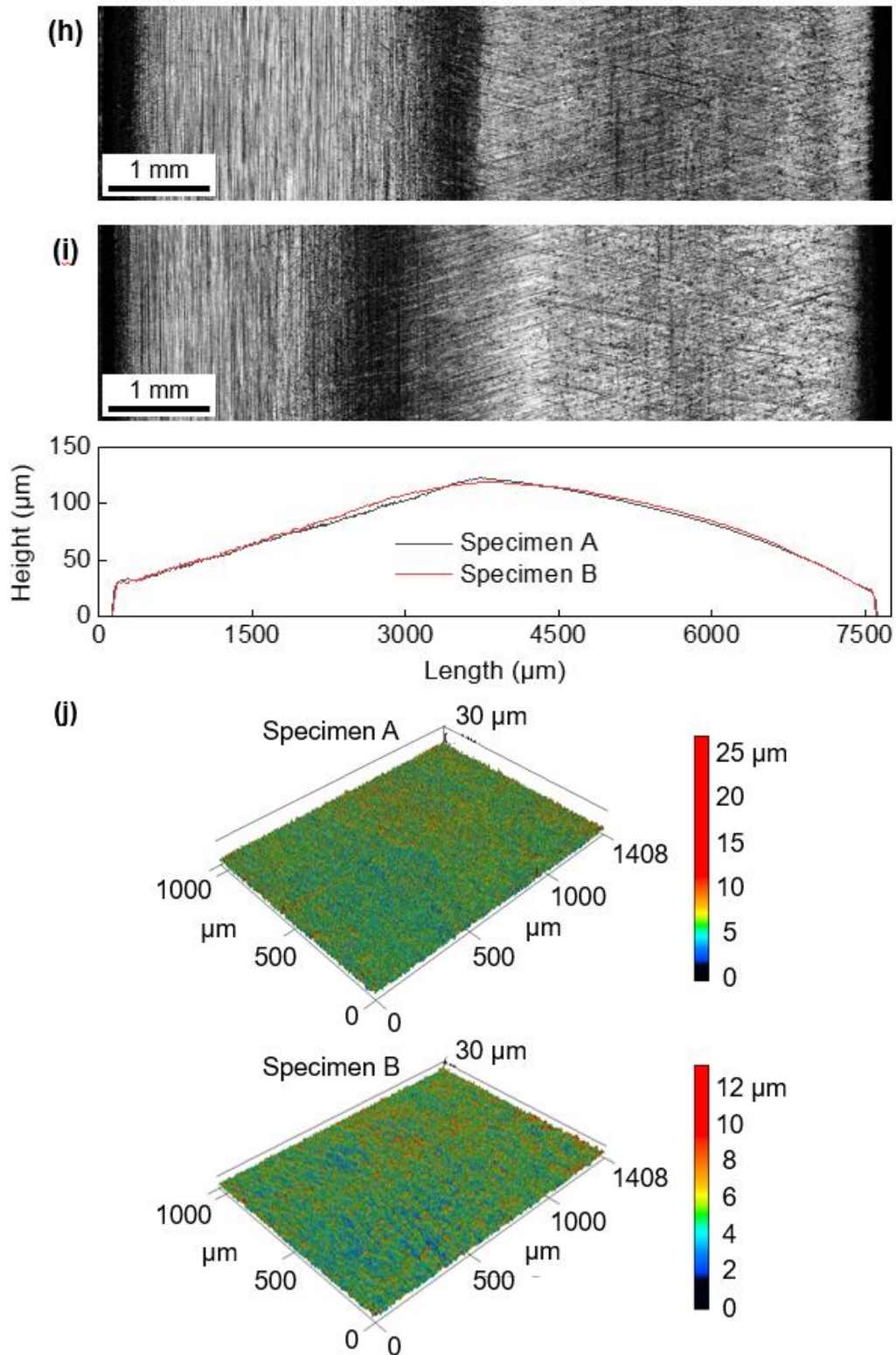


Figure 3. Cross-sectional images of specimens (a) A and (b) B, SEM images of interface of specimens (c) A and (d) B, (e) hardness, (f) load-displacement curve of coating, (g) porosity of coating, images of surface of specimens (h) A and (i) B corresponding with cross-sectional profile, (j) three-dimensional images of specimens A and B.

2.2 Methods

2.2.1 Scratch adhesion test

In this work, the adhesion between Cr-diamond coating and base materials of specimens A and B was measured using a scratch adhesion test. The scratch adhesion test model is used in this work developed by Bull and Rickerby [16]. The work of adhesion or interfacial fracture energy is calculated by determining the critical force where the coating is separated from the substrate, which means adhesion failure. The relationship between the work of adhesion and the critical force can be obtained from the equation (Eq):

$$L_C = \frac{\pi d^2}{8} \left(\frac{2EW}{t} \right)^{1/2} \quad (1)$$

L_C is the critical force, d is the scratch width, E is the elastic modulus of coating, W is the work of adhesion, and t is the coating thickness. Also, the coating thickness should be less than 50 μm for applicability of the scratch model [15].

Figure 4(a) shows the scratch specimen used in this work. The piston ring specimens for the scratch adhesion test were cut into small pieces with the dimension of $8 \times 3 \times 10.5$ mm (width \times length \times height) by using a cutting machine (IsoMet® 1000 Precision Cutter, Buehler, Illinois, USA). The cut piston ring pieces were mounted in compression mounting powder (Red Phenolic Mounting Powder, Allied, California, USA) by using a compress hot mounting machine (SimpliMet® 1000 Automatic Mounting Press, Buehler, Illinois, USA) and exposed the cross-section to measure the thickness of the coating layer during the polishing process. Then, the mounted specimens were polished

by using a polishing machine (DualPrep 3™ Grinder/Polisher, Allied, California, USA) and abrasive papers (Silicon Carbide Plain Back Disc-08", Allied, California, USA) with the 320, 600, 800, 1200, 2000 of grit sizes in order from small grit size to large grit size until the thickness of Cr-diamond coating layer is reduced to about 50 μm. The polishing process was done after polishing with suspensions (Dialube Diamond Suspensions, Allied, California, USA) with the progression of grit size was 3 μm and 1 μm. The thickness of the coating layers after the polishing process was not uniform because of the interface's curvature between the coating and the substrate. Therefore, after polishing, the average thickness of the coating layer was determined at randomly selected five different locations on the cross-section of five specimens. The average thickness of the Cr-diamond coating layer of specimens A and B is $45.15 \pm 5.60 \mu\text{m}$ and $44.59 \pm 9.76 \mu\text{m}$, respectively (mean \pm 1 standard deviation). The arithmetic average surface roughness of the Cr-diamond coating of specimens A and B obtained from laser scanning confocal microscopy data at three locations of five specimens at scan size $1408 \times 1056 \mu\text{m}$ were determined about $0.39 \pm 0.10 \mu\text{m}$ and $0.38 \pm 0.13 \mu\text{m}$, respectively (mean \pm 1 standard deviation).

The indenter used in this work is a diamond indenter (Rockwell C Diamond Indenter, Eisen, Shiga, Japan) with a spherical tip with a radius of 200 μm, elastic modulus of 1140 GPa, the hardness of 80 GPa, and ideally surface roughness. Fig. 4(a) shows the photograph of the indenter along with an example of three-dimensional laser scanning microscope images. The experimental setup photographs for the scratch tester used in this work was shown in Fig. 4(a). The diamond indenter moves under a progressive load, which increases continuously from 90 to 430 N with the constant speed

at 0.24 mm/s to make 5 mm of scratch length. As the diamond indenter scratches on the specimens, the friction force signal was monitored by a sensor. The indenter penetrates through the coating layer and presses down the substrate, which leads to the change of friction coefficient. The critical force is the normal force where the failure occurs. The average work of adhesion obtained from scratches on five specimens of each piston ring specimen following the above test parameters. The obtained results are applied to Eq. (1) to determine the work of adhesion.

In this work, different techniques for the determination of the critical force have been implemented [14,17]:

- Laser scanning confocal microscope image: Microscopic observation allows the determination of critical force and adhesion quality by examining the nature of failure mode and the extent of damage.
- Residual depth of scratch track: The depth of scratch track during scratch process is shown in the cross-sectional profile of the scratch track. At the failure point, the depth of scratch track is equivalent to the average thickness of the coating layer.
- Change the friction coefficient: The friction coefficient of the indenter-coating pair and indenter-substrate pair are quite different. Therefore, there is a change in friction coefficient when the substrate is uncovered.

2.2.2 Pin-on-reciprocating test

The friction and wear behavior of the Cr-diamond coated piston ring under oil lubrication was investigated using a pin-on-reciprocating tribo-tester. The photograph of the plate specimen used in this work is shown in Fig. 4(b). The piston ring specimens for

the pin-on-reciprocating test were cut from piston rings A and B into pieces with the dimension of $8 \times 10 \times 10.5$ mm (width \times length \times height). Chromium steel balls (Cr steel balls) were used as counterparts for sliding against piston ring specimens. Cr steel ball with a radius of 1 mm was used because of high hardness and wear resistance; therefore, the ball's wear was expected to be small. The cross-sectional profile of ball specimens was measured using a laser scanning confocal microscope before the experiment. The average radius of the balls was determined from the surface profile of the balls obtained from the laser scanning confocal microscopy data to be 1.08 ± 0.001 mm (mean \pm 1 standard deviation). The arithmetic average surface roughness of the balls was obtained from five locations with a scan size of 344×258 μ m, was about 0.11 ± 0.004 μ m (mean \pm 1 standard deviation). Fig. 4(b) shows the photograph of the ball glued on the holder, along with an example of three-dimensional laser scanning confocal microscopy images. After the ball was polished to make a flat surface, the ball's hardness was determined using the micro Vickers hardness tester. Hardness indentation was performed on randomly selected five different locations at 0.1 kgf with a dwell time 20 s. The results were determined by using the confocal microscope. The average hardness of the ball was calculated to be 921 ± 6 HV (mean \pm 1 standard deviation).

The photograph of the experimental setup of the pin-on-reciprocating tester in this work is shown in Fig. 4(b). The tests were performed with 3 mm of the stroke of the reciprocating motion at a constant rotating speed of 120 rpm, and sliding speed was calculated to be 0.012 m/s. A sensor recorded the number of cycles. All experiments were performed for 20,000 cycles; therefore, the sliding distance was calculated at about 120m. The normal force is applied by dead weight, the varied normal force (10 N, 20 N, 30 N

and 40 N) which corresponded to a contact pressure of 2.05 to 3.26 GPa for specimen A-Cr steel ball contact and 2.08 to 3.30 GPa for specimen B-Cr steel ball contact, were calculated by the sphere on plane Hertzian contact model. The friction force data was picked up using a load cell. The oil lubricant was used in this work is a commercial marine diesel engine oil (GulfSea Power MDO 4012, Kukdong, Kyongsangnam-do, Korea). The viscous index of this oil was 100. The viscosity was 144.8 cSt at 40 °C and 14.68 cSt at 100 °C, respectively. The lubricant was delivered to the contact area at one time before the experiment, just enough for boundary lubrication. The experiments were repeated at least three times for each condition; therefore, the results of the friction coefficient, wear volume and wear rate were the average values. Before the experiments, the balls and plates were cleaned by Isopropyl Alcohol (IPA) and ultrasonication in 1h to remove impurities. All experiments were performed in ambient conditions (25 °C, 40% relative humidity). After the tests, the balls' wear volume was calculated by comparing the cross-sectional profile obtained from laser scanning confocal microscope images before and after the test. The wear volume of wear tracks formed on the plates was carefully observed using a laser scanning confocal microscope. The average cross-sectional height profiles were taken in all areas of the wear track. The wear volume was calculated by multiplying the cross-sectional area of the wear track and the length of the wear track. The wear rate of the plate was calculated by the wear volume divided by normal force-multiplying with the sliding distance. The degree of wear of the balls and disks were quantitatively determined based on Archard's wear law.

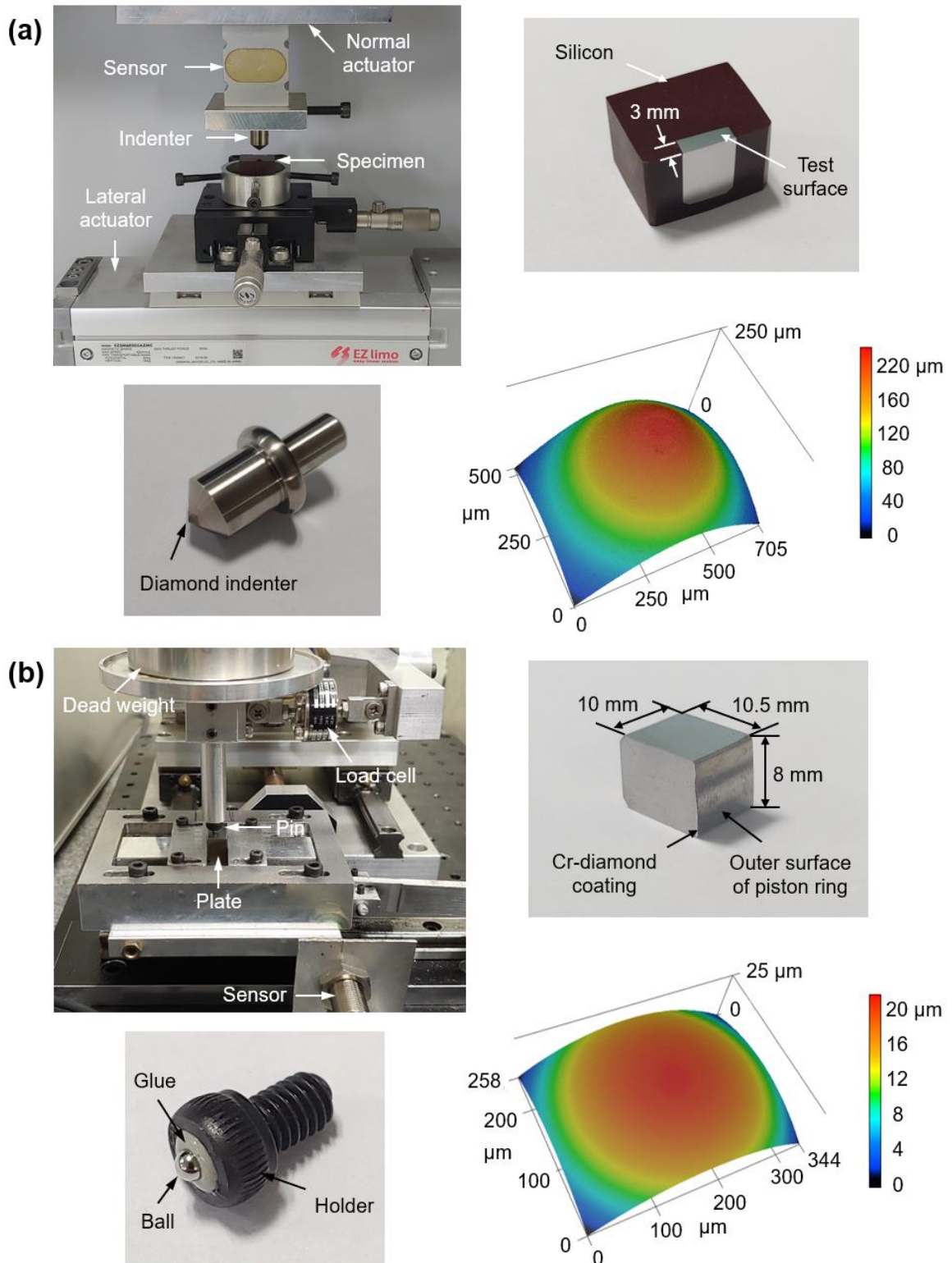


Figure 5. Photograph of (a) scratch adhesion tester, scratch specimen, indenter, and three-dimensional image of indenter, (b) pin-on-reciprocating tribo-tester, plate specimen, pin specimen and three-dimensional of the Cr steel ball.

3. RESULTS AND DISCUSSION

3.1 Adhesion characteristics

Figures 5(a) and (b) show the scratch track image along with the cross-sectional profile, normal force, lateral force, and friction coefficient profile of specimens A and B. The average thickness of the coating of specimens A and B shown in the figure is $47.95 \pm 3.91 \mu\text{m}$ and $33.16 \pm 7.49 \mu\text{m}$, respectively. The profile of the friction coefficient of both specimens shows a clear change. It results from the change of materials, which means that the indenter had penetrated the coating layer and moved down the substrate. It can be seen that there is a difference in the tendency of friction coefficient before and after the penetration of the coating layer. Besides, the friction coefficient and lateral force were unstable. It results from the continuous change of the normal force, the continuous fracture of materials during the scratch test, and the uneven thickness of the coating layer. A similar tendency of the friction force is also shown in Mouche's study for CrN coated on SiC [21]. Based on the change of friction coefficient, the critical force of the adhesion failure of specimens A and B were determined to be 220.5 N and 181.5 N of normal load, respectively. A combination of the profile of the friction coefficient to the profile of the scratch track shows that the height of the scratch track at the critical force of specimens A and B is $47.51 \mu\text{m}$ and $26.74 \mu\text{m}$, respectively. The thickness of the coating after polishing is not uniform, so it is difficult to accurately determine the coating layer's thickness at the failure point. Therefore, the height of the wear track at the failure point may be equivalent to the coating thickness there. The scratch width at the failure point of specimens A and B was carefully measured to be $363.6 \mu\text{m}$ and $250.0 \mu\text{m}$.

Figure 5(c) summarizes the coating's failure modes during the scratching process of specimen B shown in Fig. 5(b). The failure modes on two specimens were also observed on the optical images, which is the spallation by the brittle fracture of the coating material separates in front of the moving indenter. It followed a more typical brittle spallation failure mode from the research of Bull [14]. The predominant failure mechanism for Cr-diamond coating is the crack propagation to cause buckling/delamination over a large part and finally to spalling. Before the failure point, the failure mode is buckling. As the force increases, the spallation leads to the cracking on the edge of the scratch track, as shown in the optical images of both specimens, and the failure mode became the buckle spallation. Due to the great pressure in front of the indenter, when the indenter moves down, it causes the upper coating to break and splatter on the sides of the scratch track, which can be the plowing effect in front of the moving indenter. Then, the buckle spallation becomes more serious when the force increases, resulting from gross spallation. The gross spallation is seen at the end area of the scratch track. The same failure mode is also shown in Mouche's study for Cr coated on SiC [21].

The average work of adhesion of the coating layers of specimens A and B after calculating were shown in Fig. 5(d). The average work of adhesion of specimens A and B was calculated to equal to $1718.6 \pm 238.5 \text{ J.m}^{-2}$ and $2852.0 \pm 263.0 \text{ J.m}^{-2}$, respectively. It is found that the work of adhesion of specimen B is larger 66% than specimen A, which means the adhesion characteristic of Cr-diamond coating on ductile cast iron is better than grey cast iron. The reason could be the mechanical properties of ductile cast iron is better than grey cast iron. The hardness of ductile cast iron is greater about 51% than grey cast iron. Due to the higher hardness of the substrate, the pressure must be greater to

break the adhesion between the coating and the substrate. The research of Hainsworth for TiN coating also showed the effect of plastic deformation of the substrate layer on scratch performance [22]. Comparison to the results of other ceramic coatings, a very thin Cr plate coated on 25Cr3Mo3NiNb barrel steel substrate using an electroplating method, which has the interfacial fracture energy in the range of 756 J.m⁻² to 1514 J.m⁻² [23]. The SUS304 stainless steel coupons were coated with TiN by arc evaporation. It was reported that the interfacial fracture energy is 2578 J.m⁻² [15].

The results of this study are still relative due to some limitations. The original thickness of the coating layer is much larger than the limit thickness in the model of Bull and Rickerby. The interface between the coating layer and substrate is curvature, resulting in an uneven thickness after polishing. Therefore, in the future, studies with specimens whose interface of coating layer and substrate is flat, and the thickness of the coating layer is within the limitation of the model should be done.

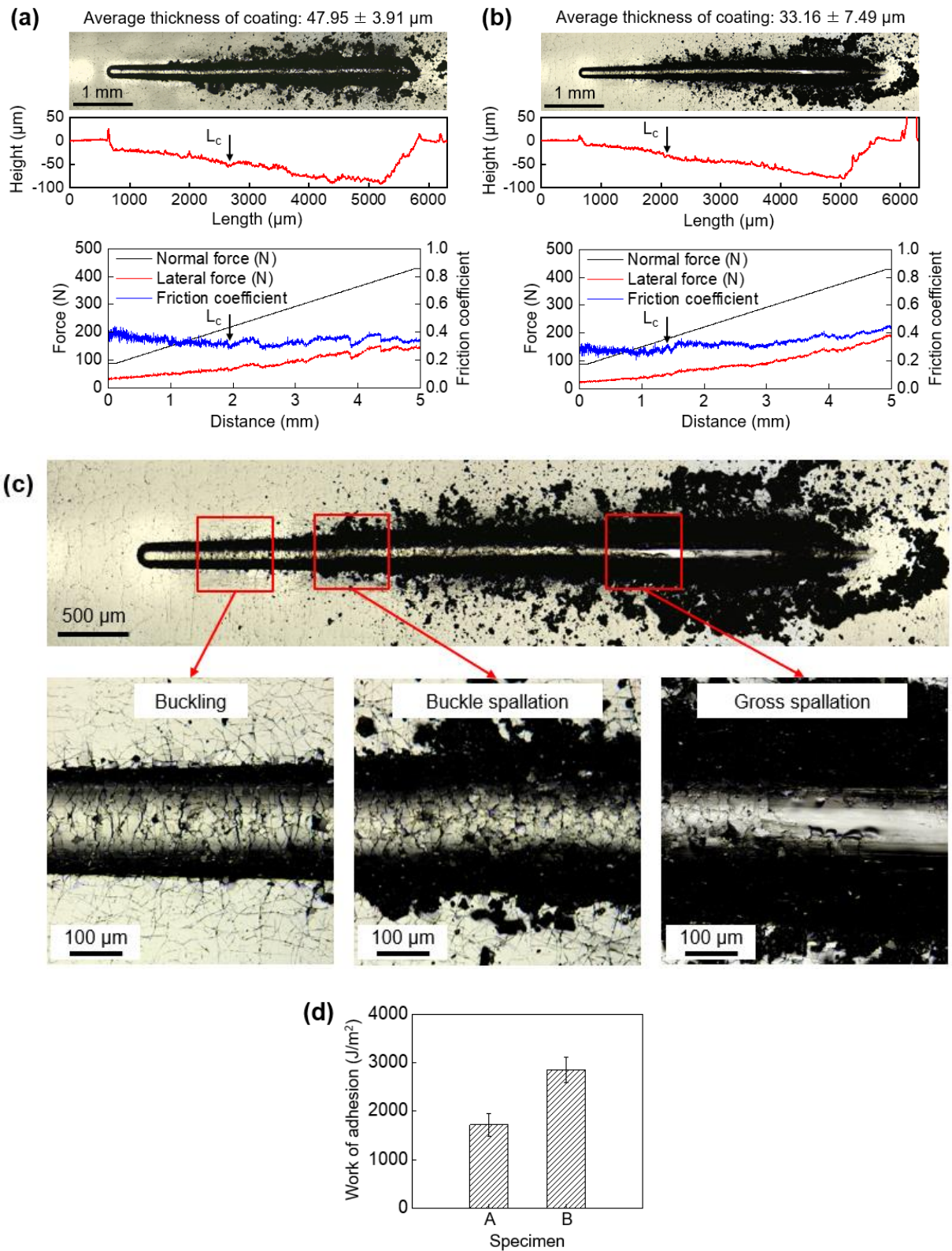


Figure 6. Optical images corresponding with cross-sectional profile of scratch track formed on specimens and friction profile of (a) specimen A and (b) specimen B, (c) failure modes, (d) work of adhesion.

3.2 Tribology characteristics

Figures 6(a) and (b) display the friction coefficient with respect to the number of cycles with variations of the normal force. At all normal force conditions, during the first 3000 cycles, the friction coefficient decreases gradually and then stabilizes until the end of the experiments. The reason may be that the initial roughness from the crosshatch pattern of the surface is worn off and then after 3000 cycles leaving the smoother surface. A similar trend in friction coefficient has been observed in the Cr piston ring [6] and CrN coating [7]. Fig. 6(c) shows the average friction coefficient under different normal forces of two specimens A and B. The average friction coefficient of specimen A under normal forces of 10 N, 20 N, 30 N and 40 N were 0.109 ± 0.001 , 0.098 ± 0.001 , 0.099 ± 0.001 and 0.098 ± 0.001 , respectively. Also, in case of specimen B the results were 0.108 ± 0.001 , 0.096 ± 0.001 , 0.096 ± 0.002 and 0.097 ± 0.001 , respectively. The average friction coefficient under the normal force of 10 N is higher about 10% than that of other normal force conditions, while the results at 20 N, 30 N, and 40 N are approximately the same. Due to the contact pressure at 10 N, it is small and not enough to wear down the initial asperities on the surface lead to maintaining the large friction. The results also indicate that the average friction coefficient of specimen A is slightly higher than that of specimen B in all normal forces; however, this difference is very small just about 1 to 3%.

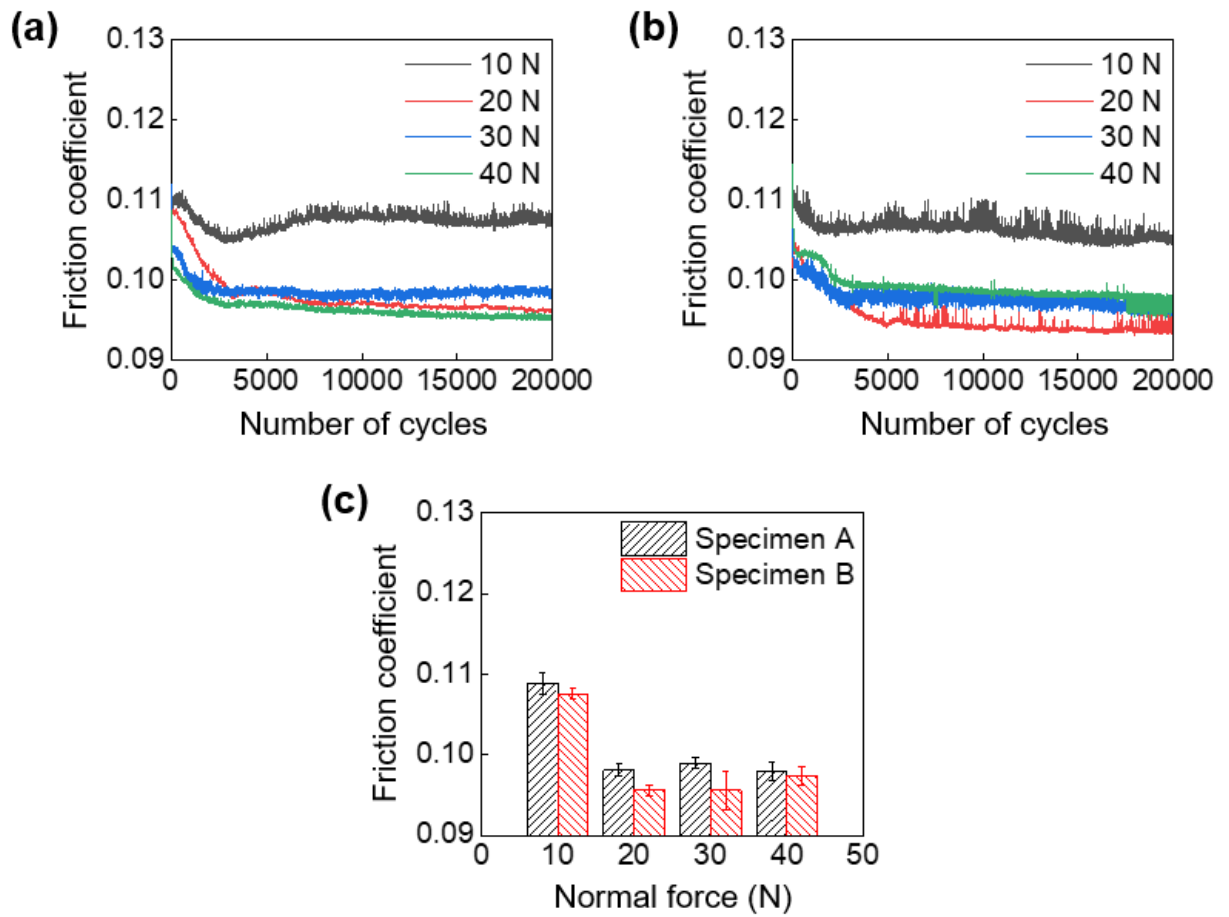


Figure 7. The friction coefficient with respect to number of cycles of different normal force of two specimens (a) A, (b) B and (c) at an average value of different normal forces.

Figure 7(a) shows optical images corresponding with cross-sectional height profiles of the Cr steel balls before and after the experiments. It was observed that the balls were flattened due to the wear. The average wear volumes and average wear rate of balls are summarized in Figs. 7 (b) and (c), respectively. The average wear volume of the balls sliding against specimen A under the normal force varies in range from 10 to 40 N were $(2.91 \pm 0.07) \times 10^{-4} \text{ mm}^3$, $(1.19 \pm 0.04) \times 10^{-4} \text{ mm}^3$, $(0.94 \pm 0.02) \times 10^{-4} \text{ mm}^3$ and $(1.03 \pm 0.03) \times 10^{-4} \text{ mm}^3$, respectively. For the balls sliding against specimen B, the results were $(2.38 \pm 0.06) \times 10^{-4} \text{ mm}^3$, $(1.06 \pm 0.02) \times 10^{-4} \text{ mm}^3$, $(0.85 \pm 0.03) \times 10^{-4} \text{ mm}^3$ and $(0.93 \pm 0.01) \times 10^{-4} \text{ mm}^3$, respectively. Therefore, the wear rate of the balls sliding against specimen A at different normal force from 10 N to 40 N after calculating from $(24.26 \pm 0.58) \times 10^{-8} \text{ mm}^3/(\text{N}\cdot\text{m})$ to $(2.60 \pm 0.27) \times 10^{-8} \text{ mm}^3/(\text{N}\cdot\text{m})$. For the balls sliding against specimen B, the results were from $(19.86 \pm 0.46) \times 10^{-8} \text{ mm}^3/(\text{N}\cdot\text{m})$ to $(1.95 \pm 0.03) \times 10^{-8} \text{ mm}^3/(\text{N}\cdot\text{m})$. Comparing the wear rate of the ball sliding against specimen B to specimen A, when the normal forces were 10 N, 20 N, 30 N and 40 N, the reduction of wear rate was 22%, 12%, 10%, and 33%, respectively. As shown in Figs. 7(b) and (c), the increasing of normal force leads to decreasing the wear volume and wear rate of the ball. The wear volume and wear rate at 10 N normal force is higher than those of other normal forces. In this case, the reason is the same as in the friction coefficient. The contact pressure at 10 N is not enough to wear the initial asperities of coating, which plays in the role the hard particles make the ball worn significantly during the sliding process. For other normal force conditions with high contact pressure, the initial asperities were removed after 3000 cycles, so ball wear is less than 10 N. In general, the wear of balls sliding against specimen A is slightly higher than that of specimen B.

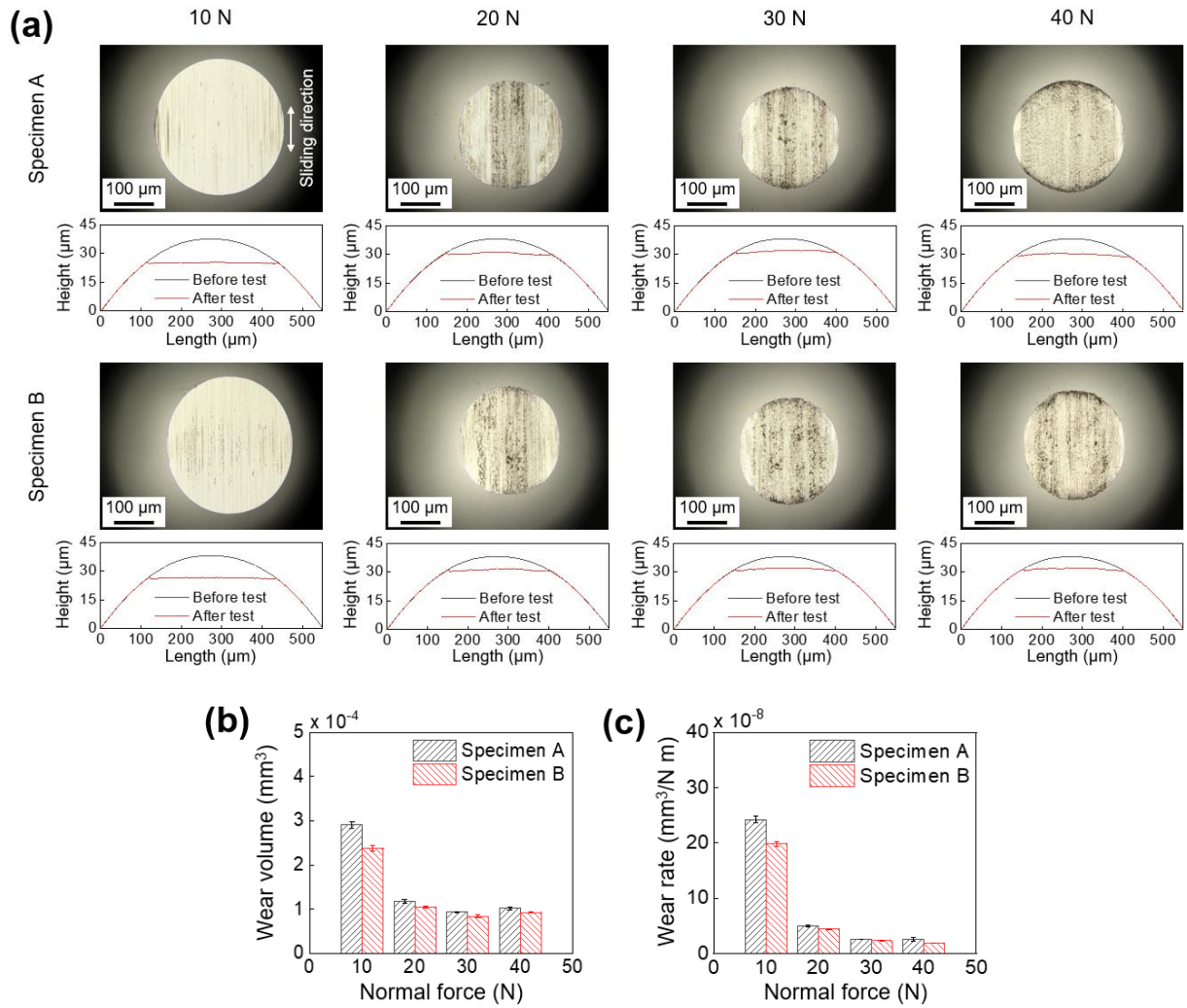


Figure 8. (a) Optical images corresponding with cross-sectional profile of wear formed on the Cr steel balls before and after test with different normal force, (b) wear volume, (c) wear rate of balls respect to normal force.

Figure 8(a) shows the optical images corresponding with cross-sectional and height profiles of wear tracks formed on specimens A and B after cleaning with different normal forces. The cross-sectional profiles of the wear tracks are also shown for comparison. According to the figure, the height of the wear track of specimens A was measured to be 0.60 μm , 1.83 μm , 1.52 μm , and 1.51 μm , while the width of the wear tracks was measured to be about 305.8 μm , 243.7 μm , 263.7 μm , and 261.2 μm as the normal force were 10 N, 20 N, 30 N and 40 N, respectively. In the experiment of specimen B performed under 10 N, the wear volume was not clear to measure, and the width of the wear scar was measured to be 306.9 μm . The height of the wear track of specimens B was 1.11 μm , 1.20 μm , and 1.27 μm , while the width of the wear tracks was 256.7 μm , 267.2 μm , and 274.0 μm as the normal force were 20 N, 30 N, and 40 N, respectively. It was observed that the width of the wear tracks of two specimens was not much different with the increasing normal force. The height of wear tracks of specimen A was slightly higher than that of specimen B. Fig. 8(b) summarizes the wear volume of plate specimens under different normal forces. The average wear volume of specimen A ranged from $(0.77 \pm 0.14) \times 10^{-4} \text{ mm}^3$ to $(8.44 \pm 0.36) \times 10^{-4} \text{ mm}^3$ as the normal force increasing from 10 N to 40 N. Also, the average wear volume of the specimen B with normal force from 20 N to 40 N ranged from $(3.78 \pm 0.15) \times 10^{-4} \text{ mm}^3$ to $(6.21 \pm 0.25) \times 10^{-4} \text{ mm}^3$. The effect of normal force on wear volume in this work follows Archard's wear law. As the normal force increases, the wear volume also increases. The average wear rate of plate specimens under different normal forces ranged from 10 N to 40 N is shown in Fig. 8(c). The average wear rate of specimen A were $(6.40 \pm 1.21) \times 10^{-4} \text{ mm}^3$, $(21.06 \pm 1.67) \times 10^{-4} \text{ mm}^3$, $(20.05 \pm 0.99) \times 10^{-4} \text{ mm}^3$, and $(17.59 \pm 0.75) \times 10^{-4} \text{ mm}^3$ as the normal

force increasing from 10 N to 40 N. The average wear rate of the specimen B was $(15.77 \pm 0.64) \times 10^{-4} \text{ mm}^3$, $(16.34 \pm 0.87) \times 10^{-4} \text{ mm}^3$ and $(12.94 \pm 0.53) \times 10^{-4} \text{ mm}^3$ as the normal force increasing from 20 N to 40 N. Under the normal force of 10 N, the wear volume of the specimens is negligible, so the wear rate is also very low compared to other normal forces. For each specimen, the normal force ranged from 20 N to 40 N, the wear rate relatively evenly. The reason may be that the wear rate is proportional to the wear volume and inversely proportional to the normal force. Also, the normal force increases, and wear volume increases, so the wear rate will not be much different. It also agrees with the tendency of the wear volume of specimens in this work. Comparing the wear rate of specimen B to specimen A, when the normal forces were 20 N, 30 N, and 40 N, the reduction of wear rate was 34%, 23%, and 36%, respectively. Generally, the results show that the wear of specimen B is slightly better than that of specimen A.

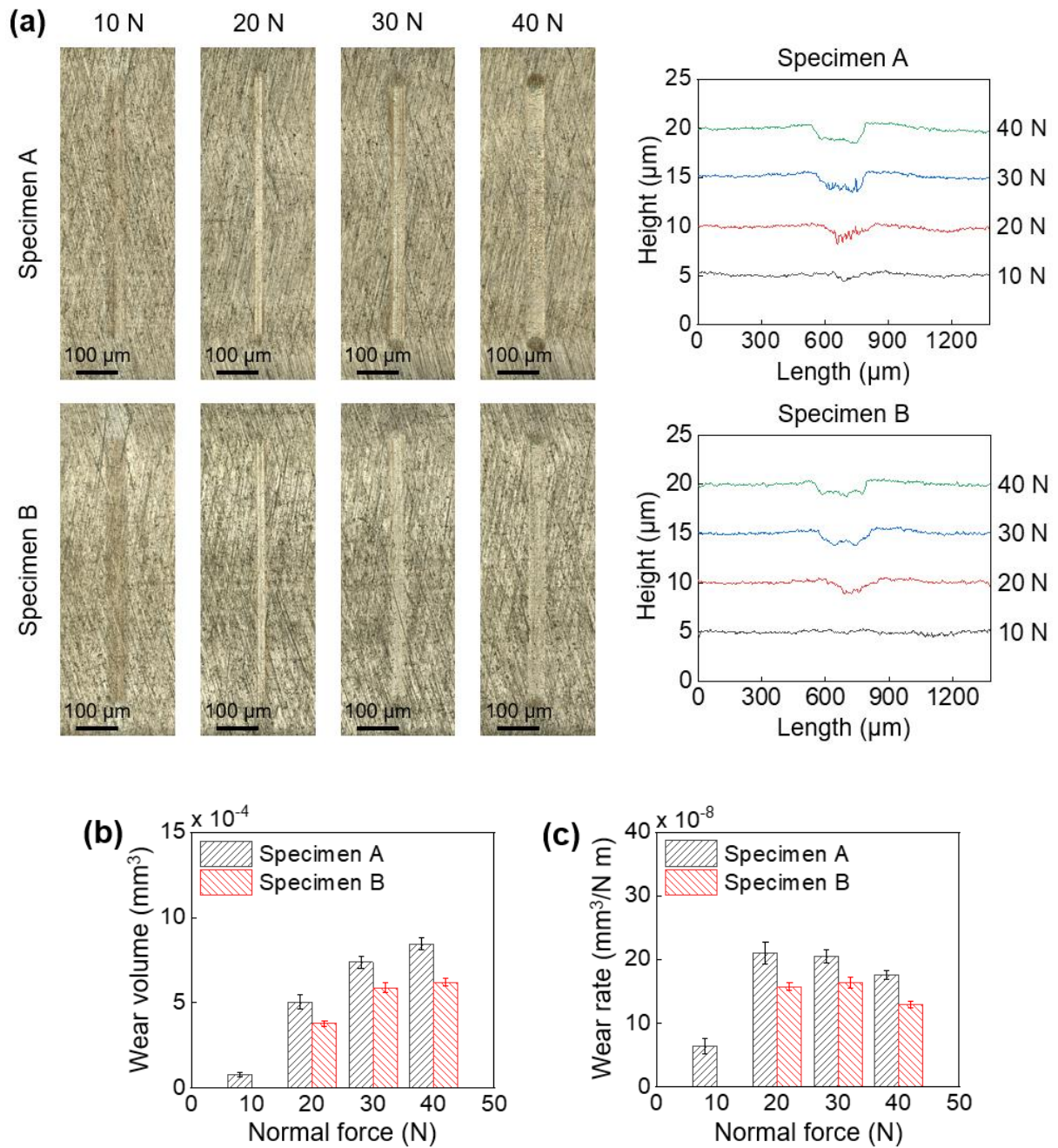


Figure 9. (a) Optical images corresponding with cross-sectional profile of wear tracks formed on the plates with different normal force, (b) wear volume, (c) wear rate of plates respect to normal force.

Figure 9(a) shows an image of the wear track formed on the specimen B under the normal force of 30 N. As shown in Fig. 9(a), the crosshatch pattern inside the wear track was almost disappeared after the experiment. The average surface roughness at five different locations with scan size $100\ \mu\text{m} \times 100\ \mu\text{m}$ inside the wear track in Fig. 9(a) was $0.17 \pm 0.01\ \mu\text{m}$. With the same determination, the average surface roughness outside the wear track was $0.29 \pm 0.03\ \mu\text{m}$. It indicates that after the experiment, the surface of the specimen was smoothed. It also means that the predominant wear mechanism of piston ring specimens in this work is smooth wear or burnishing wear. The burnishing wear is a process of single-molecule removal from the peaks of the asperities so that eventually, a perfectly smooth surface remains. Oil burn marks were also detected when the wear track was carefully observed. The reason may be that friction between the ball and specimen produces heat and the test time is relatively long enough to cause the oil and additive in the lubricant to be burned, leaving scorched oil stains on the surface of the ball and plates. Similar wear mechanisms have been observed in another study. In the research of Wenping Li and Yun Lu, the initial honing traces can be seen on the worn surface of the GDC (Cr-diamond) piston ring. The wear furrows are evenly shallower than the honing trace. The wear mechanisms of piston ring and cylinder bore are abrasive wear [10]. In the research of Shanhong Wan, the worn surface Cr–diamond piston ring is mildly damaged with shallow grooves [11]. Compared to other chromium-based coatings, in the high-speed reciprocating wear test of Cr-Al₂O₃ coated on cast-iron, the primary wear mechanism is the smooth wear, possibly by a micro-abrasion wear process [8]. Fig. 9(b) shows the high-resolution image of the worn surface of the Cr steel ball under the normal force of 30 N. The worn surface of the ball has many brown spots and

lines parallel to the sliding direction. The brown spots may be the oil burn marks, and the worn material of ball and plate specimens still have not been washed after the cleaning process still on the worn surface, and the brown lines may be the scratches. It indicates that the wear mechanism of balls in this work is adhesion wear.

The effect of the different base materials on tribological properties of coating is not clear because the thickness of the coating is much larger than the height of the wear track. All results show that friction reduction and wear resistance of specimen B is slightly better than specimen A, which may be due to the influence of the difference of surface roughness of coating. However, the data can be affected by factors such as environment and experimental conditions, so the results cannot be represented for all types of Cr-diamond coating for piston rings. Experimental conditions in this work are not the same as the actual operating conditions of the piston ring. The experiment time in this work is very short compared to the actual working time of the piston ring; therefore, the long-term test should be performed in the future to verify the results in this work. Overall, there is currently very little research on tribology characteristics of Cr-diamond coating on piston ring, so this work is expected to provide useful information for Cr-diamond studies in the future.

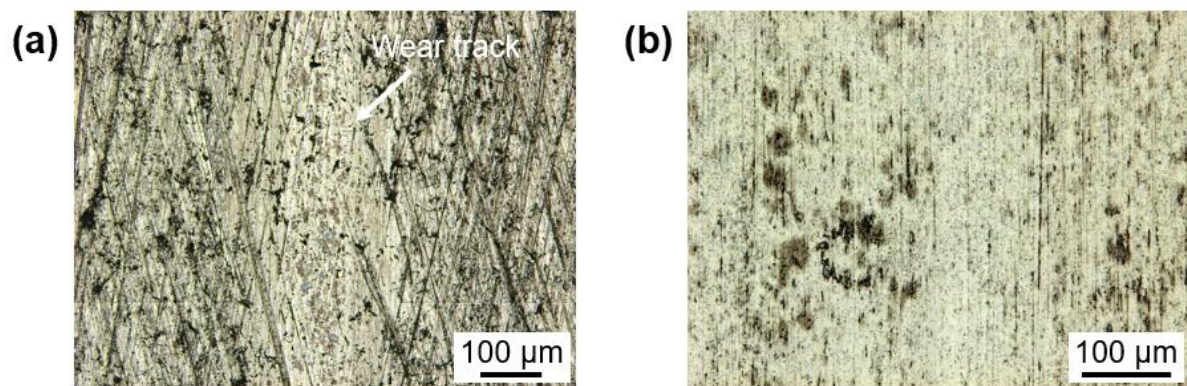


Figure 10. (a) Optical image wear tracks formed on the specimen B under 30 N of normal force, (b) high-resolution optical image of worn surface of the ball sliding against specimen B under 30 N of normal force.

4. CONCLUSIONS

In this work, the work of adhesion of Cr-diamond coating on two types of base materials, grey cast iron and ductile cast iron, was examined using a scratch test. The friction and wear behavior of Cr-diamond coating sliding against Cr steel ball under oil boundary lubrication was investigated using a pin-on-reciprocating test. The experimental results have shown the following conclusions:

1. There is no effect of base materials on the mechanical properties of the coating layers in two specimens. The hardness and elastic modulus of Cr-diamond coating on grey cast iron and ductile cast iron is similar. The surface roughness of the Cr-diamond coating on ductile cast iron was modified to be smaller 15% than grey cast iron.
2. The adhesion characteristics of Cr-diamond coating on ductile cast iron is better than grey cast iron. When ductile cast iron used as a base material, the work of adhesion increased 66 % in comparison to grey cast iron. The reason is that the mechanical properties of ductile cast iron are better than grey cast iron. The predominant failure mechanism for Cr-diamond coating is the crack propagation to cause buckling/delamination over a large part and finally to spalling. During the scratching process, the failure mode was spallation due to the high pressure in front of the indenter. This work's outcome shows the potential for using ductile cast iron as a base material for the Cr-diamond coating of a piston ring in the field condition.
3. The effect of the different base materials on friction and wear behavior of Cr-diamond coating is not clear because the coating thickness is much larger than the height of the wear track. The friction coefficient and wear rate of Cr-diamond

coating on ductile cast iron are slightly better than grey cast iron. The friction and wear rate results are not affected by the difference between the mechanical properties of coatings because hardness and elastic modulus results of coatings on two types of cast iron have been measured, which showing similarities. The reason may be surface roughness of the Cr-diamond coating on ductile cast iron was modified to be smaller 15% than grey cast iron. The best reduction of the wear rate of Cr-diamond coating on ductile cast iron compared to grey cast iron was 36% at normal force 40 N. In this work, the burnishing wear is the wear mechanism of the coating. This work's outcome may help a better understanding of the effect of surface treatment on the friction reduction and wear resistance of Cr-diamond coating, therefore providing a fundamental basis for the design of coating for enhancing the lifetimes of the piston ring.

REFERENCES

- [1] H. Yamagata, "4 - The piston ring," in *The Science and Technology of Materials in Automotive Engines*, H. Yamagata, Ed., ed: Woodhead Publishing, 2005, pp. 87-109.
- [2] M. Kapsiz, M. Durat, and F. Ficici, "Friction and wear studies between cylinder liner and piston ring pair using Taguchi design method," *Advances in Engineering Software*, vol. 42, pp. 595-603, 2011/08/01/ 2011.
- [3] K. Holmberg, P. Andersson, N.-O. Nylund, K. Mäkelä, and A. Erdemir, "Global energy consumption due to friction in trucks and buses," *Tribology International*, vol. 78, pp. 94-114, 2014/10/01/ 2014.
- [4] Y. Zhang, X. Zhang, T. Wu, and Y.-b. Xie, "Effects of surface texturing on the tribological behavior of piston rings under lubricated conditions," *Industrial Lubrication and Tribology*, vol. 68, pp. 158-169, 03/14 2016.
- [5] P. Louda, "Applications of Thin Coatings in Automotive Industry," *Journal of Achievements in Materials and Manufacturing Engineering*, vol. 24, 09/01 2007.
- [6] A. Rozario, C. Baumann, and R. Shah, "The Influence of a Piston Ring Coating on the Wear and Friction Generated during Linear Oscillation," *Lubricants*, vol. 7, p. 8, 01/14 2019.
- [7] B. Podgornik, M. Sedlaček, and D. Mandrino, "Performance of CrN coatings under boundary lubrication," *Tribology International*, vol. 96, pp. 247-257, 2016/04/01/ 2016.
- [8] P. Dearnley, E. Kern, and K. Dahm, "Wear response of crystalline nanocomposite and glassy Al₂O₃SiC coatings subjected to simulated piston ring/cylinder wall

- tests," *Proceedings of The Institution of Mechanical Engineers Part L-journal of Materials-design and Applications - PROC INST MECH ENG L-J MATER*, vol. 219, pp. 121-137, 04/01 2005.
- [9] "Coating enables piston rings to withstand high mechanical loads," *Sealing Technology*, vol. 2017, pp. 3-4, 2017/04/01/ 2017.
- [10] W. Li and Y. Lu, *The Study of Friction and Wear Capability of Piston Ring Coatings*, 2017.
- [11] S. Wan, D. Li, G. a. Zhang, A. K. Tieu, and B. Zhang, "Comparison of the scuffing behaviour and wear resistance of candidate engineered coatings for automotive piston rings," *Tribology International*, vol. 106, pp. 10-22, 2017/02/01/ 2017.
- [12] B. Q. Yang, K. Zhang, G. N. Chen, G. X. Luo, and J. H. Xiao, "Measurement of fracture toughness and interfacial shear strength of hard and brittle Cr coating on ductile steel substrate," *Surface Engineering*, vol. 24, pp. 332-336, 09/01 2008.
- [13] Z. Chen, K. Zhou, X. Lu, and Y. Lam, "A review on the mechanical methods for evaluating coating adhesion," *Acta Mechanica*, vol. 225, 02/01 2014.
- [14] S. J. Bull, "Failure mode maps in the thin film scratch adhesion test," *Tribology International*, vol. 30, pp. 491-498, 1997/07/01/ 1997.
- [15] S. J. Bull and E. G. Berasetegui, "Chapter 7 - An Overview Of The Potential Of Quantitative Coating Adhesion Measurement By Scratch Testing," in *Tribology and Interface Engineering Series*. vol. 51, S. Sinha, Ed., ed: Elsevier, 2006, pp. 136-165.
- [16] S. J. Bull, D. S. Rickerby, A. Matthews, A. Leyland, A. R. Pace, and J. Valli, "The use of scratch adhesion testing for the determination of interfacial adhesion: The

- importance of frictional drag," *Surface and Coatings Technology*, vol. 36, pp. 503-517, 1988/12/01/ 1988.
- [17] A. J. Perry, "Scratch adhesion testing of hard coatings," *Thin Solid Films*, vol. 107, pp. 167-180, 1983/09/16/ 1983.
- [18] L. L. Myagkov, K. Mahkamov, N. D. Chainov, and I. Makhkamova, "11 - Advanced and conventional internal combustion engine materials," in *Alternative Fuels and Advanced Vehicle Technologies for Improved Environmental Performance*, R. Folkson, Ed., ed: Woodhead Publishing, 2014, pp. 370-408e.
- [19] W. C. Oliver and G. M. Pharr, "An improved technique for determining hardness and elastic modulus using load and displacement sensing indentation experiments," *Journal of Materials Research*, vol. 7, pp. 1564-1583, 2011.
- [20] T. Sjögren, P. Wigren, F. Vilhelmsson, and P. Vomacka, "High performance piston rings for two-stroke marine diesel engines," *24th CIMAC World Congress on Combustion Engine Technology*, June, pp. 7-11, 01/01 2004.
- [21] P. A. Mouche, C. Ang, T. Koyanagi, P. Doyle, and Y. Katoh, "Characterization of PVD Cr, CrN, and TiN coatings on SiC," *Journal of Nuclear Materials*, vol. 527, p. 151781, 2019/12/15/ 2019.
- [22] S. V. Hainsworth and W. C. Soh, "The effect of the substrate on the mechanical properties of TiN coatings," *Surface and Coatings Technology*, vol. 163-164, pp. 515-520, 2003/01/30/ 2003.
- [23] X.-l. Li, Y. Zang, Y. Lian, M.-y. Ma, L. Mu, and Q. Qin, "An interface shear damage model of chromium coating/steel substrate under thermal erosion load," *Defence Technology*, 2020/02/08/ 2020.